RESEARCH ARTICLE

Check for updates

Confined metal centres in a symmetric cage: mono- and heterodinuclear complexes for photocatalytic hydrogen evolution

Melvin Raulin, [ID] [a,b] Federico Droghetti,[c] Davide Zeppilli,[a] Federico Begato, [ID] [a] Pradip Kumar Mondal,[d] Marzio Rancan,[e] Giulia Licini, [ID] [a,b] Laura Orian, [ID] [a] Mirco Natali*[c] and Cristiano Zonta [ID] *[a,b]

We present a supramolecular cage platform that offers modular access to distinct levels of metalation within the same confined, symmetric tris(2-pyridylmethyl)amine (**TPMA**)-based scaffold. Through a step-wise metalation strategy, well-defined homodinuclear (**ZnZn**, **CoCo**), mononuclear (**CoH$_4$**) and heterodinuclear (**CoZn**, **CoCu**) complexes can be obtained in a reproducible manner, overcoming the formation of statistical mixtures typically associated with homoditopic ligands. This molecular selectivity establishes the cage as a versatile platform to systematically compare how confinement and metal nuclearity influence reactivity in a shared supramolecular environment. As a proof of concept, the different cages were evaluated in light-driven hydrogen evolution under visible-light irradiation using $[Ru(bpy)_3]^{2+}$ as photosensitizer and ascorbate as sacrificial electron donor, revealing the mononuclear **CoH$_4$** complex as the most active catalyst. DFT calculations suggest that its enhanced activity arises from a confined second-sphere proton relay provided by the protonated, non-coordinated **TPMA** moiety. Beyond this case study, these findings establish a versatile platform for probing structure–function relationships in confined catalysts.

Introduction

Metalloenzymes achieve complex transformations by positioning one or more metal centres in confined, well-organized environments, where cooperation and second-sphere interactions govern reactivity.[1] Inspired by these natural architectures, supramolecular chemistry has increasingly focused on reproducing such confined metal pockets using synthetic ligands, macrocycles, and cages.[2,3] By controlling the spatial arrangement and microenvironment of metal sites, these systems aim to explore how confinement shapes reactivity pathways, enabling second-sphere effects or cooperative inter-actions that are not generally accessible with conventional complexes.[4] Within this context, dinuclear metal complexes featuring ditopic ligands have attracted attention due to their distinctive electronic, binding, and catalytic properties.[5] Macromolecular ligands such as macrocycles and cages offer a particularly promising platform for designing these systems.[6–8] Through their intrinsic cavities, these architectures can provide a confined and preorganized coordination sphere that modulates the reactivity of embedded metal centres. This structural control can also enable beneficial features such as proton relays,[9] intramolecular folding,[10] or water preorganization reminiscent of enzyme active sites,[11] ultimately enhancing catalytic efficiency.

These considerations highlight a broader synthetic challenge: symmetric ditopic ligands can in principle host mononuclear, homodinuclear or heterodinuclear species, but selectively accessing each state remains extremely demanding. Macromolecular architectures that can stabilize such well-defined metalation states are rare yet particularly valuable, as they enable direct comparison of distinct reactivity regimes within a single confined scaffold. Heterodinuclear systems can combine complementary coordination environments within a single cavity and exhibit cooperative effects with applications in biomimetic catalysis, small-molecule activation, and

[a]Department of Chemical Sciences, University of Padova, via F. Marzolo 1, 35131 Padova, Italy. E-mail: cristiano.zonta@unipd.it

[b]CIRCC – Consorzio Interuniversitario per le Reattività Chimiche e la Catalisi, via C. Ulpiani 27, 70126 Bari, Italy

[c]Department of Chemical, Pharmaceutical and Agricultural Sciences (DOCPAS), University of Ferrara, via L. Borsari 46, 44121 Ferrara, Italy. E-mail: mirco.natali@unife.it

[d]Elettra-Sincrotrone Trieste, S.C.p.A., S. S. 14 – km 163, 5 in Area Science Park, 34149, Basovizza, Trieste, Italy

[e]Institute of Condensed Matter Chemistry and Technologies for Energy, National Research Council (CNR) c/o Department of Chemical Sciences, University of Padova, via F. Marzolo 1, 35131 Padova, Italy

multi-electron processes.[12] In parallel, selectively stabilizing a mononuclear species in a symmetric ditopic ligand is also compelling, as the confined geometry can accentuate second-sphere interactions and other cavity-mediated effects not typically accessible to conventional complexes.[13] Achieving such selectivity, however, remains challenging with symmetric homoditopic ligands, where metal scrambling and statistical distributions often prevent the isolation of well-defined species. While strategies such as asymmetric ligands,[14,15] stepwise assembly of building blocks,[16] or bridging motifs[17] have shown some success, examples of either mononuclear or heterodinuclear cages derived from symmetric homoditopic ligands remain scarce and mostly limited to isolated cases.[18–21]

In this context, platforms that allow controlled access to both mononuclear and heterodinuclear states are especially valuable, as they not only overcome synthetic challenges but also provide a unique comparative framework to disentangle how confinement governs reactivity, whether through cooperative metal–metal effects or through second-sphere interactions. We have recently developed a novel approach to access a hydrolytically stable chiral molecular cage, *S*-1, based on the cobalt (II) tris(2-pyridylmethyl)amine **TPMA** motif through a synthetic strategy involving imine dynamic covalent chemistry combined with [3,3] diaza-Cope rearrangement.[22–24] This water-soluble architecture has been shown to efficiently coordinate two identical metal ions, Zn(II) and Co(II), through its two **TPMA** units resulting in the corresponding homodinuclear complexes **ZnZn** and **CoCo**. These species have found applications in chiral dicarboxylic acids recognition and in light-driven hydrogen photosynthesis, respectively.[9,24] The **CoCo** cage is representative of the broader family of cobalt polypyridyl HER catalysts, known for their abundance and ability to function under aqueous conditions.[25] What remains much less explored, however, is how confinement and precise metalation state within a supramolecular scaffold impact their reactivity.

In this study, we present a sequential metalation strategy that enables selective access to mononuclear (**CoH₄**) and heterodinuclear (**CoZn**, **CoCu**) complexes within this symmetric cage scaffold. This approach represents a rare example of well-defined mono- and heterodinuclear cages derived from a symmetric homoditopic ligand, overcoming the scrambling issues typically associated with such systems. The access to these distinct metalation states provides a rare opportunity to assess how confinement impacts reactivity. We therefore used photocatalytic hydrogen evolution under aqueous conditions as a model transformation, complemented by DFT calculations that highlight the involvement of second-sphere proton transfer.

Results and discussion

Homodinuclear complexes

As previously described, the cage *S*-1 coordinates two equivalents of Co(II) or Zn(II) to afford the dinuclear complexes **CoCo**

and **ZnZn**.[9,24] In the present work, we additionally obtained single crystals suitable for X-ray diffraction by slow evaporation of a water–DMSO solution, providing additional structural confirmation of these species. The structures revealed closely related three-dimensional arrangement sharing almost identical cell parameters as well as bond lengths and angles (Fig. 1b and S37, S39, Tables S6, S7). In both structures, the two **TPMA** units adopt an opposite propeller conformation, resulting in a C_3 symmetry (Fig. 1b). Each metal centre adopts a distorted trigonal bipyramidal geometry, coordinated by four nitrogen atoms from the **TPMA** ligand and one chloride anion oriented towards the interior of the cage. These chlorides are expected to be labile and readily substituted under the aqueous photocatalytic conditions employed, and are therefore omitted from the schematic representation for clarity.[26,27] The M···M and M–Cl···Cl–M distances are 9.7 Å and 5.1 Å, respectively (Table S6). Three DMSO molecules occupy each cage window (Fig. S37 and S39). The packing of the cages in the solid state forms a honeycomb-like porous framework (Fig. 1b and S38).

Mononuclear complexes

Upon monitoring **ZnZn** formation by ^{1}H NMR spectroscopy, a transient intermediate species was observed in solution. A titration of *S*-1 with increasing equivalents of zinc chloride in a 1:1 mixture of deuterated acetonitrile and water revealed a gradual decrease in the signals of the free cage, accompanied by the appearance of new signals attributed to an intermediate species (Fig. 1a). Simultaneously, the signals corresponding to the dinuclear **ZnZn** complex began to emerge. Throughout the titration, all three species (free *S*-1, the intermediate, and **ZnZn**) were clearly observed, pointing to a stepwise coordination process.

The new signals suggest that the two **TPMA** units within the cage become chemically non-equivalent upon coordination of a single zinc ion, consistent with the formation of a mononuclear complex. At higher zinc equivalents, this species was fully converted into the **ZnZn** complex. To further support this assignment, a parallel titration was performed using the triflate salt of *S*-1 instead of its chloride analogue (Fig. S35 and S36). In this case, the signals of the intermediate species appeared more distinctly split, providing clearer evidence that the two **TPMA** moieties are chemically differentiated. This observation supports the assignment of the intermediate as a mononuclear complex in which only one metal centre is bound, while the second coordination site remains unoccupied.

A comparable trend was observed during the titration of *S*-1 with cobalt(II) chloride. Despite the paramagnetic nature of the cobalt(II) centre, the intermediate, mononuclear species **CoH₄** was identifiable in the 0–20 ppm region of the ^{1}H NMR spectrum. Upon further addition of cobalt, these signals gradually decreased as the formation of the paramagnetic **CoCo** complex progressed. Notably, in contrast to zinc, cobalt coordination occurred at a significantly slower rate, allowing exclusive observation of the mononuclear intermediate in solution when one equivalent of cobalt salt was added with no
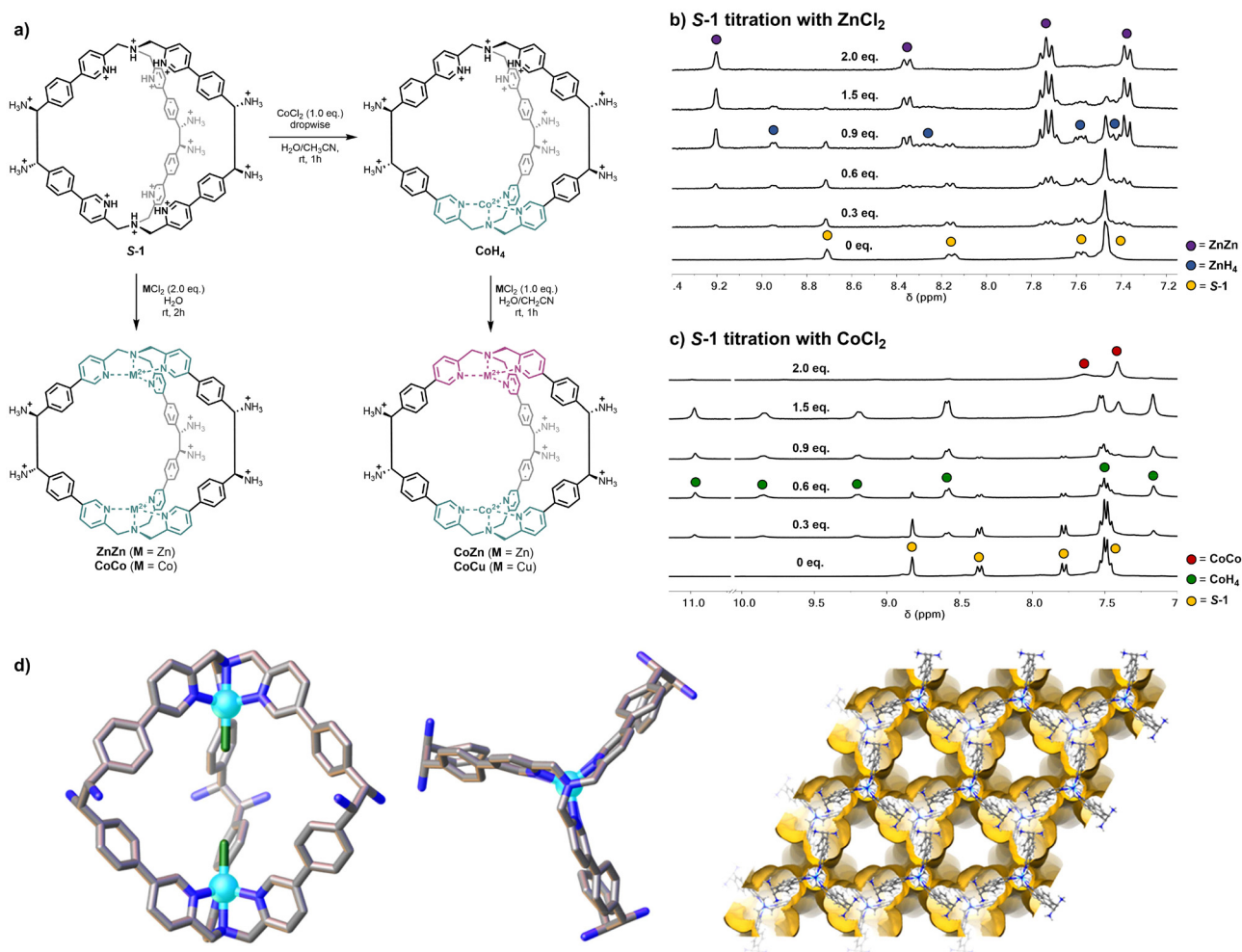
Fig. 1 (a) Reaction scheme for the synthesis of mono-, homo- and heterodinuclear chiral cages from cage **S-1**. Chloride ligands have been omitted in the schematic representation for clarity. (b) and (c) ^{1}H NMR (300 MHz, 298 K, CD$_3$CN/D$_2$O) titrations spectra of **S-1** with increasing amounts of ZnCl$_2$ and CoCl$_2$, respectively. (d) Side and top views of the **CoCo** cage as determined by single-crystal X-ray diffraction and associated voids within the honeycomb-like porous framework (probe radius: 1.2 Å). Hydrogen atoms, Cl$^-$ anions and solvent molecules are omitted for clarity. Color code: Co, cyan; N, blue; Cl, green; C, grey; voids outside, yellow; voids inside, dark yellow. **ZnZn** cage structure is displayed in the SI, Fig. S39.

detectable signals of either free **S-1** or the dinuclear **CoCo** complex. This observation indicates a non-statistical distribution of products and suggests a highly selective and kinetically controlled formation of the 1 : 1 complex. The intermediate remained stable in solution for at least 8 hours (Fig. S29), allowing straightforward characterization by NMR spectroscopy.

Heterodinuclear complexes

As shown by the titration studies, the mononuclear cobalt complex **CoH$_4$** can be obtained selectively by slow addition of one equivalent of CoCl$_2$ to the cage ligand. Building on this result, we extended this stepwise strategy by introducing a second metal centre. Addition of one equivalent of ZnCl$_2$ to the preformed **CoH$_4$** complex led to the formation of a heterodinuclear **CoZn** cage. More in detail, monitoring the reaction by ^{1}H NMR revealed the appearance of a new set of signals corresponding to two chemically distinct **TPMA** environments, with equal integration, consistent with a heterodinuclear

complex (Fig. S16). This assignment was supported by ESI-MS analysis, which confirmed the presence of the **CoZn** species (Fig. S19). The **CoZn** cage proved stable in solution, with the characteristic signals of the heterodinuclear species remaining predominant after two weeks at room temperature, as determined by ^{1}H NMR analysis (Fig. S30). A slight decrease in peak intensities was observed over this period, accompanied by the appearance of additional signals attributed to homodinuclear **CoCo** and **ZnZn** species. However, the **CoZn** cage remained the dominant species, indicating good solution stability.

A similar approach was applied to access the **CoCu** heterodinuclear cage. However, due to the paramagnetic nature of both cobalt(ɪɪ) and copper(ɪɪ), the formation of this species could not be monitored by ^{1}H NMR spectroscopy. In this case, mass spectrometry provided the primary evidence for successful heterometallation (Fig. S25); however, the presence of minor amounts of homometallic species in equilibrium cannot be excluded, and the isolation of a fully pure

CoCu cage cannot be unambiguously claimed under these conditions.

Aqueous hydrogen photocatalysis

With this series of metal-containing cages in hand, we explored the potential influence of "cage functional asymmetry" on the catalytic activity of the Co(II)-**TPMA** site for light-driven hydrogen evolution in water. This study was conducted in comparison with our previous works on similar complexes.[9,28–30] In these related systems, the photochemical cycle was shown to proceed *via* reductive quenching of the excited $[Ru(bpy)_3]^{2+}$ photosensitizer by ascorbate, followed by fast electron transfer to the cobalt centre. Specifically, the photocatalytic performances of freshly prepared **ZnZn**, **CoCo**, **CoH₄**, **CoZn**, and **CoCu** were evaluated under visible-light irradiation in aqueous acetate buffer (1 M, pH = 5) containing 0.5 mM $[Ru(bpy)_3]^{2+}$ as photosensitizer and 0.1 M ascorbate as sacrificial electron donor (Fig. 2). Each catalyst was tested at varying loadings, and catalytic activities were normalized to the total cobalt content to ensure valid comparisons (see Table S1 for the corresponding TON, TOF and QE values).

The homodinuclear **ZnZn** complex showed negligible catalytic activity, as expected for a redox-inactive system. Similarly, control experiments with the empty cage **S-1** showed hydrogen evolution activity comparable with that of a blank sample without any added catalyst (Table S2), confirming that the catalytic activity originates from the Co(II) centres rather than the organic framework. In contrast, all cobalt-containing cages, **CoCu**, **CoCo**, **CoZn**, and **CoH₄** exhibited clear hydrogen evolution activity. Among the dinuclear species, **CoCu** consistently showed the lowest performance (QE of 1.7% and 1.4% at [Co] =

100 and 50 μM, respectively), while **CoCo** and **CoZn** displayed similar kinetic profiles. For these latter, a slight inversion of trend was observed depending on cobalt concentration: **CoZn** performed marginally better at 50 μM than **CoCo** (QE = 1.9% *vs.* 1.8%; TON = 86 *vs.* 76), whereas at 100 μM, **CoCo** showed a higher initial efficiency (QE = 3.7% *vs.* 2.6%), but **CoZn** ultimately reached a slightly higher cumulative yield (TON = 68 *vs.* 63). Taken together, these results indicate that the nature of the second metal centre can influence the catalytic efficiency of the Co(II) site, although the effect is subtle. These variations among dinuclear species may reflect differences in second-sphere interactions within the confined cavity, such as electrostatic effects,[31] coordination dynamics,[32] or water structuring,[33] as proposed in related multimetallic systems.

Notably, the mononuclear cobalt complex **CoH₄** exhibited the highest catalytic efficiency of the series, with hydrogen evolution rates appreciably higher than those observed for the dinuclear species and QEs up to 6% (see Table S1). While dinuclear catalysts might *a priori* be expected to benefit from the presence of two metal centres through cooperative or synergistic effects between neighboring sites,[34,35] as demonstrated in various molecular and heterogeneous systems, no such enhancement is observed at the level of overall catalytic activity here, indicating that effective intermetallic cooperation is not operative within the present cage architecture. For comparison, in our previous study on related Co-**TPMA** half-cages, the best catalyst reached a QE of 7.4% at comparable conditions, highlighting that the confined proton-relay motif remains the decisive factor for enhanced activity.[9] A plausible rationale for this result is that the uncoordinated **TPMA** arm, protonated under the reaction conditions, may facilitate second-sphere proton transfer through a hydrogen-bonded water network confined within the cage cavity. This hypothesis is consistent with supramolecular preorganization mechanisms previously proposed in related synthetic and enzymatic systems.[34,35] Similar conclusions were reached in our previous study on related Co-**TPMA** cages, where transient absorption experiments confirmed that electron transfer from the photosensitizer to the cobalt centre is rapid and not rate-limiting.[9] This provided further evidence that proton transfer is the key step modulated by the confined environment, an aspect we further explored through DFT calculations as detailed below.

### Computational insights into second-sphere proton transfer within Co(II) cage catalysts

To gain deeper insights into the catalytic trends observed experimentally, particularly the superior activity of the mononuclear **CoH₄** cage and the role of second-sphere interactions in modulating activity, density functional theory (DFT) calculations were carried out to model proton transfer and oxidation processes within the cavity of the cages (level of theory: SMD-PBE1PBE-D3(BJ)/6-311+G(d,p),def2-TZVP//SMD-PBE1PBE-D3(BJ)/6-31G(d),SDD).

We first examined the mononuclear **CoH₄** species, which features a cobalt-**TPMA** centre and a second, non-coordinated **TPMA** unit. A fully optimized structure of the cage was computed, including a hydrogen-bonded cluster of three water
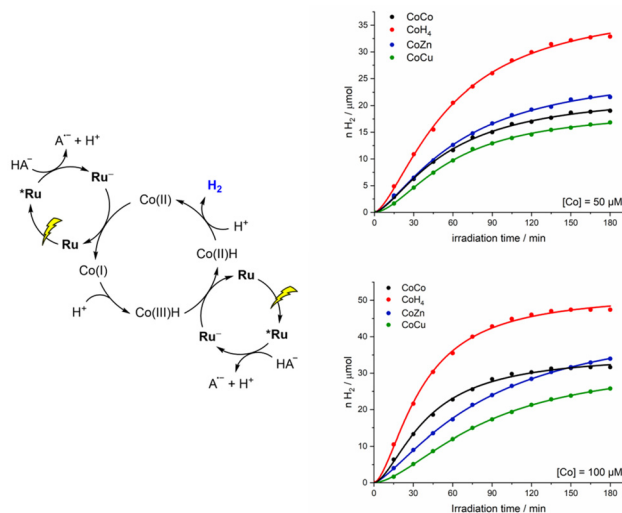
Fig. 2 (Left) Schematic representation of the proposed mechanism of photochemical H₂ evolution with Ru = $[Ru(bpy)_3]^{2+}$ as the sensitizer and HA⁻ = ascorbate as the sacrificial electron donor; (right) kinetics of H₂ formation upon continuous irradiation (460 nm LED) of 1 M acetate buffer solutions (pH 5) containing 0.5 mM $[Ru(bpy)_3]^{2+}$, 0.1 M ascorbate, and the cage: (top right) [Co] = 50 μM, (bottom right) [Co] = 100 μM.
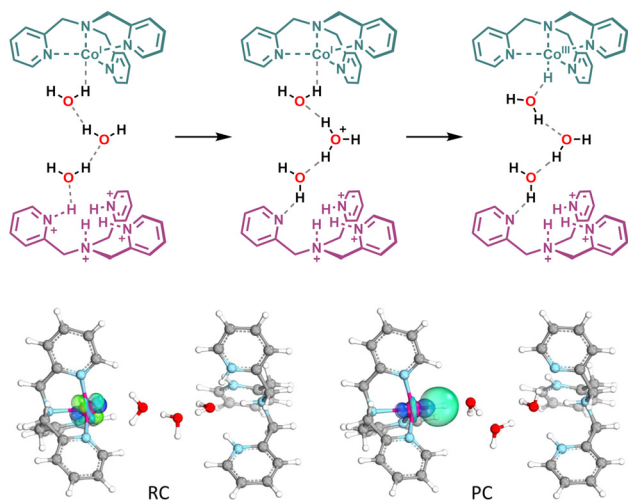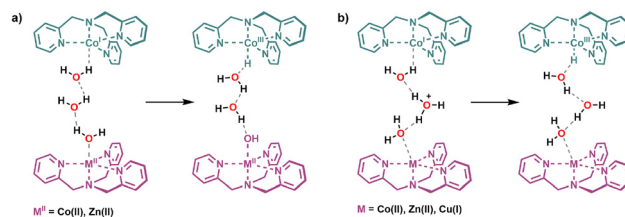
Fig. 3 Protonation and oxidation of Co(I) to Co(III)−H in the mononuclear **CoH$_4$** system. Structures of reactant (RC) and product (PC) complexes with α (blue) and β (green) spin IBOs involved in the process. Color code: Co, fuchsia; N, blue; O, red; C, grey; H, white. Level of theory: SMD-PBE1PBE-D3(BJ)/def2-TZVP//SMD-PBE1PBE-D3(BJ)/6-31G(d),SDD.

Scheme 1 Schematic representation of the two protonation/oxidation pathways of Co(I) to Co(III)−H, as considered in the DFT study. (a) Proton relay *via* a hydrogen-bonded network of water molecules inside the cavity. (b) Acid-assisted pathway mediated by a hydronium ion.

molecules positioned between the metal centre and the protonated tripodal ligand. To reduce computational effort, a minimal model was designed by deleting the cage's arms while maintaining the **TPMA** ligands frozen in space (see Computational methods). This configuration is illustrated in Fig. 3, where a proton originating from a pyridinium group is shuttled through the water network to the Co(I) centre, accompanied by formal oxidation to Co(III)−H. This process implies electron donation from Co(I), which can be evaluated by looking at the involved Intrinsic Bond Orbitals (IBOs) of the reactant and product complexes (Fig. 3). Both α (blue) and β (green) spin IBOs are initially localized on the metal as atomic d orbitals; then, they both become part of the Co−H σ bond, supporting the description of the oxidation of Co(I) to Co(III). However, only the β spin IBO (green) is mostly localized on the H atom, while the other IBO remains localized on the metal. This indicates a strong radical character of H in the product complex, explaining also the high spin contamination (see Computational methods). The computed energy profile (Fig. S40) reveals two transition states: the first (TS1) at 8.1 kcal mol^{-1} leads to a hydronium-stabilized intermediate (7.9 kcal mol^{-1}), and the second (TS2) at 19.6 kcal mol^{-1} affords the product complex, which lies 14.1 kcal mol^{-1} above the reactant. Thus, in the mononuclear cage **CoH$_4$** the protonation of Co(I) to yield Co(III)−H is feasible but overall endergonic, setting the stage for comparison with the dinuclear systems.

The same approach was extended to homo- and heterodinuclear species. In the presence of Co(II), Zn(II) or Cu(I) as second metal centers, proton abstraction occurs at the water molecule next to the metal (Scheme 1a), resulting in hydroxide coordination, while the proton is shuttled directly to Co(I). In contrast to the mononuclear cage, no stable intermediate was located, and the process was found to be significantly less favor-

able. For full-cage optimizations, the reaction energy of the product complex lies at 28.0 kcal mol^{-1} for **CoZn** and 29.0 kcal mol^{-1} for **CoCo**, compared to only 9.6 kcal mol^{-1} for **CoH$_4$** (Table S5). For **CoCu**, optimization of the product was not successful due to the intrinsic instability of Cu(I)OH, indicating that this pathway is not viable for this system. These results indicate that the introduction of a second metal perturbs the hydrogen-bonding network and penalizes proton transfer, thereby suppressing the reactivity of the confined Co(I) site.

An alternative pathway involving a pre-formed hydronium ion within the confined water cluster was also evaluated (Scheme 1b). This scenario, consistent with acidic aqueous conditions, led to lower reaction energies with values of 6.5 kcal mol^{-1} for **CoZn**, 7.8 kcal mol^{-1} for **CoCo**, and 8.6 kcal mol^{-1} for **CoCu** (Table S5). In this case, the relative trend **CoZn** < **CoCo** ≈ **CoCu** is preserved. However, these values are not directly comparable to **CoH$_4$**, as pathway (b) assumes the prior formation and stabilization of a hydronium ion within the cavity; the associated energetic and entropic costs are not captured by the reported electronic energies. Thus, pathway (b) should be regarded as an acid-assisted scenario that provides qualitative trends among dinuclear species rather than a direct standard of comparison to the mononuclear case.

In the particular case of **CoCu**, the cage was modeled in the Co(I)/Cu(I) oxidation state, since the electrochemical reduction of Co(II) to Co(I) implies a similar reduction of Cu(II) to Cu(I). For this model, both reactions were tested, but any attempt to optimize the product of Scheme 1a was unsuccessful, likely due to the instability of Cu(I)OH, which prevents its formation. Thus, only the second reaction (Scheme 1b) is feasible for the **CoCu** case. The computed reaction energy (Table S5) is consistent with the experimental observation that **CoCu** is the least active species among the dinuclear metal systems studied.

Although minimal models tend to overestimate reaction barriers, optimizations of the full cage indicate a stabilizing effect arising from cavity confinement. In particular, when the product complex of the mononuclear **CoH$_4$** complex is optimized within the complete cage, the reaction energy becomes less disfavored (Table S5).

This behavior is consistent with enthalpic compensation mechanisms commonly observed in confined catalytic environments, including enzymatic systems modeled with constrained minimal structures.[36]

Taken together, these results provide a consistent computational rationale for the experimentally observed superior performance of the mononuclear **CoH4** complex.

The presence of a non-coordinated, protonated **TPMA** moiety in **CoH4** enables an efficient second-sphere proton relay through the confined water cluster, whereas the introduction of a second metal perturbs this network and penalizes the key Co–H bond-forming step. The slightly more favorable energetics calculated for Zn(II) relative to Co(II) and Cu(I) also correlate with the subtle relative performance of the **CoCo**, **CoZn** and **CoCu** catalysts.

Conclusions

In this study, we have addressed the synthetic challenge of selectively accessing distinct metalation states within a **TPMA**-based symmetric cage by developing a stepwise strategy that affords the mononuclear **CoH4** complex alongside heterodinuclear **CoZn** and **CoCu** species. This represents a rare example of controlled mono- and heterodinuclear metalation in such architectures, thereby overcoming the scrambling issues typically associated with symmetric homoditopic ligands and enabling a direct comparison of reactivity regimes within a single supramolecular platform. Photocatalytic tests in light-driven hydrogen evolution revealed that **CoH4** exhibits superior activity relative to its dinuclear counterparts, consistent with the proposed role of the protonated, non-coordinated **TPMA** moiety in facilitating proton transfer within the confined cavity. DFT calculations further support this interpretation, suggesting that second-sphere proton relays and confined water networks modulate reactivity, and that these features are perturbed upon introduction of a second metal. By linking structural control to catalytic performance, this work illustrates how confinement can be harnessed to disentangle the contributions of mono- *versus* dinuclear environments in supramolecular catalysis. Looking ahead, this metalation strategy could in principle be extended to other **TPMA**-binding metal combinations and transformations, thereby advancing the design of functional confined catalysts in supramolecular chemistry and biomimetic catalysis. More broadly, this approach provides a framework for designing confined catalysts where cooperative or second-sphere effects can be systematically probed and exploited, in analogy to enzymatic active sites.

Author contributions

The manuscript was written through contributions of all authors. All authors have given approval to the final version of the manuscript.

Conflicts of interest

There are no conflicts to declare.

Data availability

The data underlying this study is available in the supplementary information (SI). Supplementary information: materials and methods, experimental procedures, ^{1}H NMR, UV-vis, FT-IR and HRMS spectra, XRD experimental, tables and figures. See DOI: **https://doi.org/10.1039/d5qi02424b**.

The authors have cited additional references within the SI.[37–57]

CCDC 2455177 (**CoCo**) and 2455178 (**ZnZn**) contain the supplementary crystallographic data for this paper.[58a,b]

Acknowledgements

References

1 M. Zhao, H.-B. Wang, L.-N. Ji and Z.-W. Mao, Insights into metalloenzyme microenvironments: biomimetic metal complexes with a functional second coordination sphere, *Chem. Soc. Rev.*, 2013, **42**, 8360–8375.

2 J. Meeuwissen and J. N. H. Reel, Supramolecular catalysis beyond enzyme mimics, *Nat. Chem.*, 2010, **2**, 615–621.

3 C. V. Stappen, Y. Deng, Y. Liu, H. Heidari, J.-X. Wang, Y. Zhou, A. P. Ledray and Y. Lu, Designing Artificial Metalloenzymes by Tuning of the Environment beyond the Primary Coordination Sphere, *Chem. Rev.*, 2022, **122**, 11974–12045.

4 F. Begato, G. Licini and C. Zonta, Exploiting Chirality in Confined Nanospaces, *Angew. Chem., Int. Ed.*, 2023, **62**, e202311153.

5 G. Li, D. Zhu, X. Wang, Z. Su and M. R. Bryce, Dinuclear metal complexes: multifunctional properties and applications, *Chem. Soc. Rev.*, 2020, **49**, 765–838.

6 S. Zhang, Q. Wang, L. M. Thierer, A. B. Weberg, M. R. Gau, P. J. Carroll and N. C. Tomson, Tuning Metal–Metal Interactions through Reversible Ligand Folding in a Series of Dinuclear Iron Complexes, *Inorg. Chem.*, 2019, **58**, 12234–12244.

7 K. Omoto, S. Tashiro, M. Kuritani and M. Shionoya, Multipoint Recognition of Ditopic Aromatic Guest Molecules via Ag–π Interactions within a Dimetal Macrocycle, *J. Am. Chem. Soc.*, 2014, **136**, 17946–17949.

8 T. Ouyang, H.-H. Huang, J.-W. Wang, D.-C. Zhong and T.-B. Lu, A Dinuclear Cobalt Cryptate as a Homogeneous Photocatalyst for Highly Selective and Efficient Visible-Light Driven CO2 Reduction to CO in CH_3CN/H_2O Solution, *Angew. Chem., Int. Ed.*, 2017, **56**, 738–743.

9 F. Droghetti, F. Begato, M. Raulin, G. Musiu, G. Licini, M. Natali and C. Zonta, Strong Enhancement in Cobalt(II)-TPMA Aqueous Hydrogen Photosynthesis through Intramolecular Proton Relay, *Angew. Chem., Int. Ed.*, 2024, **63**, e202408316.

10 N. Noll, T. Groß, K. Shoyama, F. Beuerle and F. Würthner, Folding-Induced Promotion of Proton-Coupled Electron Transfers via Proximal Base for Light-Driven Water Oxidation, *Angew. Chem., Int. Ed.*, 2023, **62**, e202217745.

11 N. Noll, A.-M. Krause, F. Beuerle and F. Würthner, Enzyme-like water preorganization in a synthetic molecular cleft for homogeneous water oxidation catalysis, *Nat. Catal.*, 2022, **5**, 867–877.

12 M. Hardy and A. Lützen, Better Together: Functional Heterobimetallic Macrocyclic and Cage-like Assemblies, *Chem. – Eur. J.*, 2020, **26**, 13332–13346.

13 J. M. Stauber, G. E. Alliger, D. G. Nocera and C. C. Cummins, Second-Coordination-Sphere Assisted Selective Colorimetric Turn-on Fluoride Sensing by a Mono-Metallic Co(II) Hexacarboxamide Cryptand Complex, *Inorg. Chem.*, 2017, **56**, 7615–7619.

14 S. Thoonen, S. E. Walker, D. L. Marshall, T. M. Fulloon, S. Brandon, A. I. McKay, M. J. Paterson, K. M. Mullen, J. D. Crowley, K. L. Tuck and D. R. Turner, Single-Step Synthesis of a Heterometallic [Cu2PdL4]2+ Hybrid Metal-Organic Coordination Cage, *Angew. Chem., Int. Ed.*, 2025, e202506064.

15 J. Jökel, E. Birsen Boydas, J. Wellauer, O. S. Wenger, M. Robert, M. Römelt and U.-P. Apfel, A CuICoII cryptate for the visible light-driven reduction of CO2, *Chem. Sci.*, 2023, **14**, 12774–12783.

16 N. Eren, F. Fadaei-Tirani and K. Severin, Stepwise synthesis of heterotrimetallic FeII/PdII/AuI coordination cages, *Inorg. Chem. Front.*, 2024, **11**, 3263–3269.

17 J.-L. Pierre, P. Chautemps, S. Refaif, C. Beguin, A. El Marzouki, G. Serratrice, E. Saint-Aman and P. Rey, Imidazolate-Bridged Dicopper(II) and Copper-Zinc Complexes of a Macrobicyclic Ligand (Cryptand). A Possible Model for the Chemistry of Cu—Zn Superoxide Dismutase, *J. Am. Chem. Soc.*, 1995, **117**, 1965–1973.

18 M. Kuritani, S. Tashiro and M. Shionoya, Heterodinuclear Metal Arrangement in a Flat Macrocycle with Two Chemically- Equivalent Metal Chelating Sites, *Inorg. Chem.*, 2012, **51**, 1508–1515.

19 T. Ouyang, H.-J. Wang, H.-H. Huang, J.-W. Wang, S. Guo, W.-J. Liu, D.-C. Zhong and T.-B. Lu, Dinuclear Metal Synergistic Catalysis Boosts Photochemical CO2-to-CO Conversion, *Angew. Chem., Int. Ed.*, 2018, **57**, 16480–16485.

20 M. Rancan, M. Rando, L. Bosi, A. Carlotto, R. Seraglia, J. Tessarolo, S. Carlotto, G. H. Clever and L. Armelao, Dynamic lanthanide exchange between quadruple-stranded cages: the effect of ionic radius differences on

kinetics and thermodynamics, *Inorg. Chem. Front.*, 2022, **9**, 4495–4505.

21 J. Biswas, K. Kulbir, P. Bhardwaj, S. Ghosh, S. C. Sahoo, U.-P. Apfel and P. Kumar, Acid-catalyzed Transformation of Nitrite to Nitric Oxide on Copper(II)-Cobalt(II) Centers in a Bimetallic Complex, *Chem. – Eur. J.*, 2024, **30**, e202402295.

22 M. Raulin, G. Licini and C. Zonta, Tris(2-pyridylmethyl) amines-based metal complexes as versatile scaffold in catalysis, *Coordination Chemistry Reviews*, 2026, DOI: **10.1016/j.ccr.2025.217417**.

23 C. Bravin, E. Badetti, G. Licini and C. Zonta, Tris(2-pyridyl-methyl)amines as emerging scaffold in supramolecular chemistry, *Coord. Chem. Rev.*, 2021, **427**, 213558.

24 F. Begato, R. Penasa, K. Wurst, G. Licini and C. Zonta, Combining Imine Condensation Chemistry with [3,3] Diaza-Cope Rearrangement for One-Step Formation of Hydrolytically Stable Chiral Architectures, *Angew. Chem., Int. Ed.*, 2023, **62**, e202304490.

25 F. Droghetti, F. Lucarini, A. Molinari, A. Ruggi and M. Natali, Recent findings and future directions in photosynthetic hydrogen evolution using polypyridine cobalt complexes, *Dalton Trans.*, 2022, **51**, 10658–10673.

26 J.-W. Wang, H.-H. Huang, J.-K. Sun, T. Ouyang, D.-C. Zhong and T.-B. Lu, Electrocatalytic and Photocatalytic Reduction of CO2 to CO by Cobalt(II) Tripodal Complexes: Low Overpotentials, High Efficiency and Selectivity, *ChemSusChem*, 2018, **11**, 1025–1031.

27 S. D. Kettenmann, F. R. Louka, E. Marine, R. C. Fischer, F. A. Mautner, N. Kulak and S. S. Massoud, Efficient Artificial Nucleases for Mediating DNA Cleavage Based on Tuning the Steric Effect in the Pyridyl Derivatives of Tripod Tetraamine-Cobalt(II) Complexes, *Eur. J. Inorg. Chem.*, 2018, **20–21**, 2322–2338.

28 M. Natali, E. Badetti, E. Deponti, M. Gamberoni, F. A. Scaramuzzo, A. Sartorel and C. Zonta, Photoinduced hydrogen evolution with new tetradentate cobalt(II) complexes based on the TPMA ligand, *Dalton Trans.*, 2016, **45**, 14764–14773.

29 E. Benazzi, F. Begato, A. Niorettini, L. Destro, K. Wurst, G. Licini, S. Agnoli, C. Zonta and M. Natali, Electrocatalytic hydrogen evolution using hybrid electrodes based on single-walled carbon nanohorns and cobalt(II) polypyridine complexes, *J. Mater. Chem. A*, 2021, **9**, 20032–20039.

30 P. Zardi, J. Piękoś, A. C. Bravin, K. Wurst, F. Droghetti, M. Natali, G. Licini, A. Zambon and C. Zonta, Novel ligands from direct benzylic functionalisation of tris(2-pyridyl-methyl)amine, *Dalton Trans.*, 2024, **53**, 13831–13836.

31 J. Zhou, W. Nie, D. E. Tarnopol and C. C. L. McCrory, Co-Co and Co-Zn bimetallic complexes for electrocatalytic CO2 reduction: The role of interrelated intramolecular effects on activity, *Chem. Catal.*, 2024, **4**, 101006.

32 V. Singh, M. G. Robb and S. Brooker, Testing mixed metal bimetallic, and monometallic, cryptates for electrocatalytic hydrogen evolution, *Dalton Trans.*, 2025, **54**, 3165–3173.

33 V. Kunz, J. O. Lindner, M. Schulze, M. I. S. Röhr, D. Schmidt, R. Mitrić and F. Würthner, Cooperative water oxidation catalysis in a series of trinuclear metallosupra-

molecular ruthenium macrocycles, *Energy Environ. Sci.*, 2017, **10**, 2137–2153.

34 Q.-P. Zhao, W.-X. Shi, J. Zhang, Z.-Y. Tian, Z.-M. Zhang, P. Zhang, Y. Wang, S.-Z. Qiao and T.-B. Lu, Photo-induced synthesis of heteronuclear dual-atom catalysts, *Nat. Synth.*, 2024, **3**, 497–506.

35 Y.-N. Gong, S.-Q. Zhao, H.-J. Wang, Z.-M. Ge, C. Liao, K.-Y. Tao, D.-C. Zhong, K. Sakai and T.-B. Lu, A Planar-Structured Dinuclear Cobalt(II) Complex with Indirect Synergy for Photocatalytic CO2-to-CO Conversion, *Angew. Chem., Int. Ed.*, 2024, **63**, e202411639.

36 N. Noll and F. Würthner, Bioinspired Water Preorganization in Confined Space for Efficient Water Oxidation Catalysis in Metallosupramolecular Ruthenium Architectures, *Acc. Chem. Res.*, 2024, **57**, 1538–1549.

37 N. Sakashita, H. Ishikita and K. Saito, Rigidly hydrogen-bonded water molecules facilitate proton transfer in photosystem II, *Phys. Chem. Chem. Phys.*, 2020, **22**, 15831–15841.

38 M. Dalla Tiezza, F. M. Bickelhaupt, L. Flohé and L. Orian, Proton Transfer and SN2 Reactions as Steps of Fast Selenol and Thiol Oxidation in Proteins: A Model Molecular Study Based on GPx, *ChemPlusChem*, 2021, **86**, 525–532.

39 J. A. Broomhead, C. G. Young and P. Hood, Tris(2,2-Bipyridine)Ruthenium(II) Dichloride Hexahydrate, *Inorg. Synth.*, 1990, **28**, 338.

40 F. Droghetti, A. Amati, A. Ruggi and M. Natali, Bioinspired motifs in proton and CO2 reduction with 3d-metal polypyridine complexes, *Chem. Commun.*, 2024, **60**, 658–673.

41 S. P. Pitre, C. D. McTiernan, W. Vine, R. DiPucchio, M. Grenier and J. C. Scaiano, Visible-Light Actinometry and Intermittent Illumination as Convenient Tools to Study Ru (bpy)3Cl2 Mediated Photoredox Transformations, *Sci. Rep.*, 2015, **5**, 16397.

42 A. Nanthakumar, S. Fox, N. N. Murthy and K. D. Karlin, Inferences from the 1H-NMR Spectroscopic Study of an Antiferromagnetically Coupled Heterobinuclear Fe(III)–(X)–Cu(II) S = 2 Spin System (X = O2-, OH-), *J. Am. Chem. Soc.*, 1997, **119**, 3898.

43 A. Lausi, M. Polentarutti, S. Onesti, J. R. Plaisier, E. Busetto, G. Bais, L. Barba, A. Cassetta, G. Campi, D. Lamba, A. Pifferi, S. C. Mande, D. D. Sarma, S. M. Sharma and G. Paolucci, Status of the crystallography beamlines at Elettra, *Eur. Phys. J. Plus*, 2015, **130**, 1–8.

44 W. Kabsch, XDS, *Acta Crystallogr., Sect. D: Biol. Crystallogr.*, 2010, **66**, 125–132.

45 O. V. Dolomanov, L. J. Bourhis, R. J. Gildea, J. A. K. Howard and H. Puschmann, OLEX2, *J. Appl. Crystallogr.*, 2009, **42**, 339–341.

46 G. M. Sheldrick, SHELXT – Integrated space-group and crystal-structure determination, *Acta Crystallogr., Sect. A: Found. Adv.*, 2015, **71**, 3–8.

47 G. M. Sheldrick, Crystal structure refinement with SHELXL, *Acta Crystallogr., Sect. C: Struct. Chem.*, 2015, **71**, 3–8.

48 M. J. Frisch, G. W. Trucks, H. B. Schlegel, G. E. Scuseria, M. A. Robb, J. R. Cheeseman, G. Scalmani, V. Barone, G. A. Petersson, H. Nakatsuji, X. Li, M. Caricato, A. V. Marenich, J. Bloino, B. G. Janesko, R. Gomperts, B. Mennucci, H. P. Hratchian, J. V. Ortiz, A. F. Izmaylov, J. L. Sonnenberg, D. Williams-Young, F. Ding, F. Lipparini, F. Egidi, J. Goings, B. Peng, A. Petrone, T. Henderson, D. Ranasinghe, V. G. Zakrzewski, J. Gao, N. Rega, G. Zheng, W. Liang, M. Hada, M. Ehara, K. Toyota, R. Fukuda, J. Hasegawa, M. Ishida, T. Nakajima, Y. Honda, O. Kitao, H. Nakai, T. Vreven, K. Throssell, J. A. Montgomery, J. A. Montgomery Jr, J. E. Peralta, F. Ogliaro, M. J. Bearpark, J. J. Heyd, E. N. Brothers, K. N. Kudin, V. N. Staroverov, T. A. Keith, R. Kobayashi, J. Normand, K. Raghavachari, A. P. Rendell, J. C. Burant, S. S. Iyengar, J. Tomasi, M. Cossi, J. M. Millam, M. Klene, C. Adamo, R. Cammi, J. W. Ochterski, R. L. Martin, K. Morokuma, O. Farkas, J. B. Foresman and D. J. Fox, *Gaussian 16, Revision C.01, Gaussian16*, Gaussian, Inc., Wallingford, CT, 2016.

49 J. P. Perdew, K. Burke and M. Ernzerhof, Generalized Gradient Approximation Made Simple, *Phys. Rev. Lett.*, 1996, **77**, 3865–3868.

50 J. P. Perdew, K. Burke and Y. Wang, Generalized Gradient Approximation for the Exchange-Correlation Hole of a Many-Electron System, *Phys. Rev. B: Condens. Matter Mater. Phys.*, 1996, **54**, 16533–16539.

51 C. Adamo and V. Barone, Toward Reliable Density Functional Methods without Adjustable Parameters: The PBE0 Model, *J. Chem. Phys.*, 1999, **110**, 6158–6170.

52 A. D. Becke and E. R. Johnson, A Density-Functional Model of the Dispersion Interaction, *J. Chem. Phys.*, 2005, **123**, 154101.

53 S. Grimme, S. Ehrlich and L. Goerigk, Effect of the Damping Function in Dispersion Corrected Density Functional Theory, *J. Comput. Chem.*, 2011, **32**, 1456–1465.

54 D. Figgen, G. Rauhut, M. Dolg and H. Stoll, Energy-Consistent Pseudopotentials for Group 11 and 12 Atoms: Adjustment to Multi-Configuration Dirac–Hartree–Fock Data, *Chem. Phys.*, 2005, **311**, 227–244.

55 A. V. Marenich, C. J. Cramer and D. G. Truhlar, Universal Solvation Model Based on Solute Electron Density and on a Continuum Model of the Solvent Defined by the Bulk Dielectric Constant and Atomic Surface Tensions, *J. Phys. Chem. B*, 2009, **113**, 6378–6396.

56 K. Yamaguchi, F. Jensen, A. Dorigo and K. N. Houk, Spin Correction Procedure for Unrestricted Hartree-Fock and Møller-Plesset Wavefunctions for Singlet Diradicals and Polyradicals, *Chem. Phys. Lett.*, 1988, **149**, 537–542.

57 S. Fernández, F. Franco, C. Casadevall, V. Martin-Diaconescu, J. M. Luis and J. Lloret-Fillol, A Unified Electro- and Photocatalytic CO2 to CO Reduction Mechanism with Aminopyridine Cobalt Complexes, *J. Am. Chem. Soc.*, 2020, **142**, 120–133.

58 (*a*) CCDC 2455177: Experimental Crystal Structure Determination, 2026, DOI: **10.5517/ccdc.csd.cc2ndt85**; (*b*) CCDC 2455178: Experimental Crystal Structure Determination, 2026, DOI: **10.5517/ccdc.csd.cc2ndt96**.